On Modeling Evaporation of Sessile Drops

Lou Kondic, New Jersey Institute of Technology, Newark, NJ, U.S.A.
Nebojsa Murisic, University of California Los Angeles, Los Angeles, CA, U.S.A.

The Proceedings of The 2008 Annual Meeting of AIChE
Philadelphia, PA

1 Introduction

Evaporating drops and thin films have numerous applications, from nanometric photoresist films in semiconductor applications to small sessile drops used for analysis of DNA microarrays [1]. Evaporating sessile drops are particularly interesting due to nonuniform drop thickness and the presence of contact lines (separating liquid, gas and solid phase). These factors may lead to nonuniform evaporation along the liquid/gas interface, that induces temperature gradients and related Marangoni effects. The Marangoni effects are a critical ingredient in explaining important problems involving deposits, such as the well know coffee-stain problem [2] and its' numerous applications [1]. Hence, the benefits of thorough understanding of the evaporation process in sessile drops are evident.

Although the problem of an evaporating drop on a thermally conductive solid substrate appears to be rather simple, important aspects regarding this very basic process remain unknown. This is mainly due to the fact that the evaporation phenomena involves an interplay of a number of physical effects, including mass and energy transfer between the three phases, diffusion and/or convection of the vapor in the gas phase, coupled with complex physics of the contact line (see, e.g., [3, 4]). Even if one is to ignore the issues related to the contact line region and the thermal effects in the solid phase, the resulting "2-sided" model that only includes processes in the liquid and the gas phases provides a mathematical obstacle of considerable difficulty [5]. Various simplifications of the 2-sided model have surfaced over the last decade. They rely on estimating the importance of relevant physical processes, thereby reducing the complex problem to a single phase consideration (liquid or gas). However, these estimates involve quantities that are not know precisely enough.

The full 2-sided model can be first simplified by noting that the viscosity and thermal conductivity of vapor are small compared to those in the liquid. An additional assumption that the gas phase is free of convection, reduces the 2-sided model to a so called "1.5-sided" model, where only the processes in the liquid and the diffusion of vapor into surrounding gas are considered [6]. A commonly used simplification of the 1.5-sided model is achieved by assuming that the time-scale relevant to diffusion of vapor into surrounding gas is much longer than the one relevant to the phase-change [7, 8]. As a result, the processes in the liquid phase can be ignored. This approach also involves the assumption of thermodynamic equilibrium at the evaporating interface, and critically relies on the relevant thickness of the gas phase, which is unknown. As an outcome, the problem is reduced to a simple Laplace's equation for concentration of vapor in the gas phase. At this point, one may notice an electrostatic analogy of finding an electric

field (mass flux) in the exterior of a lens-shaped conductor (the drop) at a fixed potential (vapor concentration) [2, 9]. This "lens" evaporation model has been used in problems involving evaporative drops with both pinned (stationary) [7, 10] and moving contact lines [11], for evaporation of alkane drops [12], and in predicting the behavior of colloidal drops [9, 13], as well as the temperature at the liquid/gas interface [14].

On the other hand, if one shifts focus to the liquid phase, the heat diffusion through the liquid that supplies the heat to the liquid/gas interface, and the evaporation itself are the most relevant physical processes. Estimating the significance of these processes relies on the value of a single parameter, the accommodation coefficient α, which describes the probability of phase-change [5, 15]. In particular, the limit $\alpha \to 0$ leads to a reaction-limited regime, with interface at non-equilibrium, while the limit $\alpha \to 1$ leads to a (heat) diffusion-limited regime, with interface at equilibrium. Unfortunately, the value of α is not know well enough – a variety of values in a wide range $O(1) - O(10^{-6})$ have been used in literature, often with very little justification [5, 16]. If we assume that α is very small (e.g. $O(10^{-4})$), the corresponding evaporation time-scale is not only much longer than the liquid heat diffusion time-scale, but also significantly longer than the vapor diffusion time-scale [17]. As a result, the diffusion of vapor in the gas phase can be ignored, and the model is reduced to a non-equilibrium one-sided ("NEOS") evaporation model. The NEOS model has been extensively used for evaporating thin films [5, 16, 18], but only few works have applied it to the problem of evaporating drops [13, 19, 20].

Both lens and NEOS evaporation models require the use of unknown quantities, thereby making it difficult to decide which one of these two models is more appropriate. In this paper, we introduce a mathematical model for describing the evolution of drop thickness. We keep the mass flux expression explicitly in our formulation, which enables us to use both of these evaporation models. Next, we describe a set of experiments which allow us to calculate the volatility coefficients corresponding to each model. Finally, we show how our mathematical model can be used together with the experimental data to predict which evaporation model, lens or NEOS, is more suitable for describing the evolution of small deionized water (DIW) drops evaporating from smooth silicon (Si) wafers.

2 The mathematical model

The model consists of Navier-Stokes equations for liquid, coupled with the energy equations for solid and liquid, and an appropriate expression for mass flux, J. We model the solid-liquid interaction through a disjoining pressure model (van der Waals intermolecular forces – vdW), resulting in use of precursor film, and apply the lubrication approximation. More detailed description of the derivation procedure can be found in [17, 20]. In cylindrical coordinates and assuming azimuthal symmetry, we obtain the following PDE for the drop thickness $h(r,t)$

$$\frac{\partial h}{\partial t} + EJ + \frac{S}{r}\left[rh^3\left(h_{rrr} + \frac{1}{r}h_{rr} - \frac{1}{r^2}h_r\right)\right]_r - \frac{E^2}{rD}\left[rJh^3J_r\right]_r + \frac{M}{rP}\left[rh^2\left(h+\mathcal{W}\right)J_r\right]_r + \frac{M}{rP}\left[rJh^2h_r\right]_r + \frac{A}{r}\left[rh^3\left(\left(\frac{b}{h}\right)^3 - \left(\frac{b}{h}\right)^2\right)_r\right]_r + \frac{G}{r}\left[rh^3h_r\right]_r = 0\,. \tag{1}$$

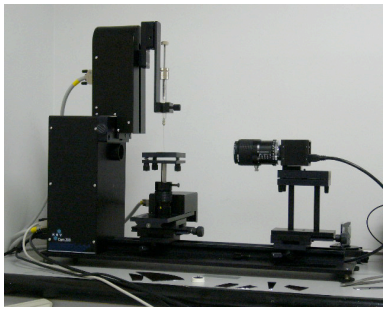

Figure 1: The goniometer: camera, syringe and the deposition platform.

The individual terms of eq. (1) represent effects due to viscosity, evaporation, surface tension, vapor recoil, Marangoni stresses (two terms), vdW forces, and gravity, respectively. The definitions of nondimensional coefficients appearing in eq. (1), as well as the list of values of physical parameters used are given in [15, 20].

The key point in eq. (1) is the mass flux, J. The details of the derivation of the expressions for $J(h)$ corresponding to lens and NEOS models are given elsewhere [17]. Here, we only list these expressions and briefly comments on their properties. The expression for J appropriate for lens model is

$$J = \frac{\chi}{h^{\lambda}}, \tag{2}$$

where χ is the volatility parameter, while the exponent λ is a function of the contact angle Θ: $\lambda = 0.5 - \Theta/\pi$ [7]. We note that according to eq. (2), J diverges at the contact line ($h \to 0$). In the case of NEOS model, the expression for J is given by

$$J = \frac{1}{h + \mathcal{W} + \mathcal{K}}, \tag{3}$$

where $\mathcal{K} = \mathcal{K}(\alpha) \propto 1/\alpha$ is the coefficient of non-equilibrium, while $\mathcal{W}$ accounts for thermal properties in the solid [16, 20]. Typically, $\mathcal{W} + \mathcal{K} \sim O(10)$ and hence, the mass flux in this case depends only weakly on h. Crucial volatility parameters χ and α are obtained from experiments which we describe next.

3 The experiments

The experiments are performed in room conditions ($298K$ and 50% relative humidity) and in open atmosphere, with minimal hindrance by undesired external convection. We use pure DIW and smooth semiconductor grade Si wafers, treated by chemical-mechanical polishing that produces surface roughness (Rms) of $0.5nm$. The drops are deposited manually using a Hamilton 1700 Series GASTIGHT syringe and allowed to evaporate freely. The temperature of the solid wafers is not controlled. The measurements are carried out using a KSV CAM200 goniometer with built-in software for analyzing the data. The goniometer consists of a horizontal platform with automated vertical and horizontal movement onto which the wafer is placed, the syringe clamp, and the camera. Figure 1 shows the complete experimental set-up. As the experiments proceed, the camera automatically captures images of the drop profile at pre-set time intervals.

The experiments were carried out repeatedly in order to ensure the reproducibility. All experiments involve $4.9\mu l$ DIW drops and focus on the time interval $[0, 106s]$. With the exception of a brief interval ($< 2s$) immediately after the deposition, during which the drop shape changes rapidly, the evolution is relatively slow. Hence, the images are taken at $8s$ intervals.

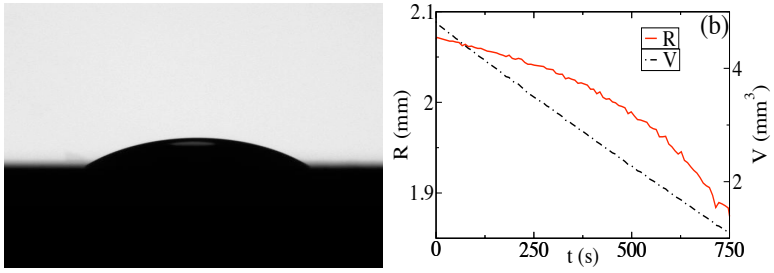

Figure 2: (a) Snapshot of evaporating DIW drop on Si substrate; (b) Volume and radius of the drop as a function of time (experimental results).

The built-in software examines each individual image, first checking if the spherical cap approximation can be applied to the drop profile. Based on this approximation, the software outputs the radius R, height at the center of the drop H, and the contact angle Θ, enabling us to calculate the drop volume and surface area corresponding to each image. Therefore, we are able to monitor the evolution of these parameters as the experiment proceeds. Figure 2 shows an image captured by the camera (a) and typical evolution of drop volume and radius (b). In agreement with previous works, Figure 2(b) shows linear decrease of volume for the considered time interval [7, 9, 21]. However, we find neither significant stick-slip motion, nor contact line pinning, which were documented in [7]. Possible reasons for this difference are smoothness of Si wafers and purity of DIW which we use. Furthermore, the experimental data indicates that, except for aforementioned brief sequence, the value of the contact angle changes only slightly during the considered time interval. Therefore, in our model, moving contact lines and fixed contact angle are considered.

The extraction of volatility coefficients, χ and α, from the experimental data is accomplished in the following manner. The considered time interval $[0, 106s]$ is divided into short subintervals, with endpoints corresponding to the time instants $t_1, t_2, ..., t_N$, for which experimental data are available. This procedure allows us to compute the evaporation rate ${J^{rate}}_k$, corresponding to each subinterval $[t_k, t_{k+1}]$, $k = 1, 2, ..., N$, by using the experimental data for volume and surface area of the drop at the endpoints of these subintervals. In particular, ${J^{rate}}_k$ is found by using the change of volume and surface area during subinterval $[t_k, t_{k+1}]$. The crucial observation is that the calculated value of ${J^{rate}}_k$ has to match the integral of an appropriate expression for mass flux J, integrated over experimentally recorded surface of the drop (spherical cap) at the time instant t_{k+1}

$$ {J^{rate}}_k = \int_{S_{k+1}} J \, dS = \int_0^{2\pi} \int_0^{R_{k+1}} J(r)\Phi(r) r \, dr \, d\vartheta, \tag{4} $$

where R_{k+1} is the radius of the drop and $\Phi(r)$ is the Jacobian corresponding to the drop surface at time t_{k+1}. The expression for $J(r)$, depending on which evaporation model is considered, is

the mass flux given by either eq. (2) or eq. (3), rewritten as a function of r, the radial distance from the center of the drop toward the contact line.

In particular, for the lens model, we have

$$J^{rate}{}_k = \int_0^{2\pi}\int_0^{R_{k+1}} \frac{\chi_k {d_0}^{\lambda} J_{sc} r}{\left(\sqrt{{B_{k+1}}^2 - r^2} - d_{k+1} + b\right)^{\lambda}} \sqrt{1 + \frac{r^2}{{B_{k+1}}^2 - r^2}}\, dr\, d\vartheta, \tag{5}$$

where parameter set $(R_{k+1}, B_{k+1}, d_{k+1})$ describes the spherical cap at time t_{k+1}, d_0, J_{sc} and b are the appropriate length-scale, mass flux scale, and non-dimensional precursor thickness respectively, while χ_k is the volatility coefficient appropriate throughout the time interval $[t_k, t_{k+1}]$ (for details see [22]). Integrating with respect to ϑ while treating χ_k as constant yields

$$\chi_k = \frac{J^{rate}{}_k}{2\pi {d_0}^{\lambda} J_{sc} B_{k+1} I_{k+1}}, \tag{6}$$

where I_{k+1} denotes the integral

$$I_{k+1} = \int_0^{R_{k+1}} \frac{r}{\sqrt{{B_{k+1}}^2 - r^2}\left(\sqrt{{B_{k+1}}^2 - r^2} - d_{k+1} + b\right)^{\lambda}}\, dr, \tag{7}$$

which is calculated numerically for each $k = 1, ..., N-1$. Having calculated χ_k's we obtain the value for χ corresponding to the time interval $[0, 106s]$ by averaging over all χ_k's.

In the case of NEOS model, eq. (4) leads to

$$J^{rate}{}_k = \int_0^{2\pi}\int_0^{R_{k+1}} \frac{d_0 J_{sc} r \sqrt{1 + \frac{r^2}{{B_{k+1}}^2 - r^2}}}{\sqrt{{B_{k+1}}^2 - r^2} - d_{k+1} + b + d_0\left(\mathcal{K}(\alpha_k) + \mathcal{W}\right)}\, dr\, d\vartheta, \tag{8}$$

where α_k is the accommodation coefficient valid in the time interval $[t_k, t_{k+1}]$, treated as constant. While the factorization of χ_k from eq. (5) is achieved in a straightforward manner, the nature of eq. (8) does not allow equivalent factorization of α_k, making the calculation of α_k a bit more complex. Integration of eq. (8) with respect to ϑ leads to

$$J^{rate}{}_k = 2\pi d_0 J_{sc} B_{k+1} \Xi_{k+1}(\alpha_k), \tag{9}$$

where $\Xi_{k+1}(\alpha)$ is given by

$$\Xi_{k+1}(\alpha_k) = \int_0^{R_{k+1}} \frac{r}{\sqrt{{B_{k+1}}^2 - r^2}\left(d_0\left(\mathcal{K}(\alpha_k) + \mathcal{W}\right) - d_{k+1} + b\right) + {B_{k+1}}^2 - r^2}\, dr. \tag{10}$$

The problem of solving for α_k is therefore reformulated into a minimization problem

$$\alpha_k = \min_{\alpha_k \in [10^{-6}, 1]} \Gamma(\alpha_k), \tag{11}$$

where $\Gamma(\alpha_k)$ is given by

$$\Gamma(\alpha_k) = \left| \frac{J^{rate}{}_k}{2\pi d_0 J_{sc} B_{k+1}} - \Xi_{k+1}(\alpha_k) \right|, \tag{12}$$

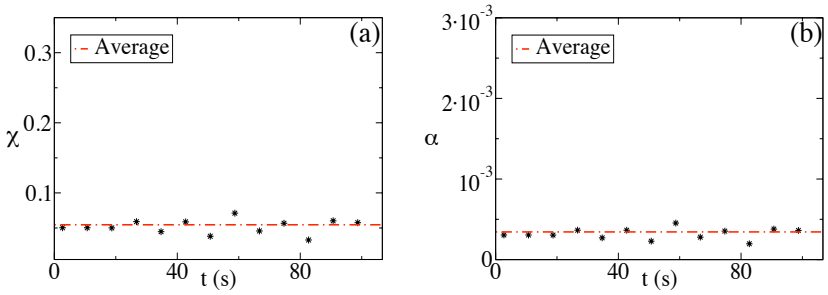

Figure 3: Volatility coefficients for the DIW/Si configuration for the first $106s$. Stars indicate calculated values, dashed lines indicate corresponding average value. (a) lens model: $\chi = (5.5 \pm 1) \cdot 10^{-2}$; (b) NEOS model: $\alpha = (3.4 \pm 0.7) \cdot 10^{-4}$.

and is solved numerically for all k. As in the case of χ, the value of α valid for the whole time interval $[0, 106s]$ is obtained by averaging over all α_k's.

We expect that the outlined method for calculating volatility coefficients χ and α is more accurate than simply using the measured dryout time to estimate the mass flux, as it is well-know that at late stages of evolution, the evaporation rate may be reduced [21]. Figure 3 shows the volatility parameters χ and α over a time interval of $106s$. While some noise exists in our experimental data, we note that it is evident from Figure 3 that the values of both volatility coefficients do not exhibit tendency for growth or decay as evaporation proceeds, and remain close to their respective mean values. Therefore, the assumption that these volatility coefficients are constant is reasonable.

Finally, in order to ensure the quality of our experimental data, we apply the method outlined in this section to the experimental data from [7]. In particular, we focus on data regarding small water drops evaporating on a glass cover slip. Although the experimental set-up in [7] differs from the one considered here, namely, it involves pinned contact lines, we obtain $\chi = 5.1 \cdot 10^{-2}$ and $\alpha = 3.1 \cdot 10^{-4}$, which are in excellent agreement with the results for χ and α obtained from our own data. Therefore, we have an independent confirmation that our experimental results are reasonably accurate.

4 The comparison of evaporation models and discussion

Having calculated the volatility coefficients for the two evaporation models, all necessary ingredients for our mathematical model are in place. In order to compare the two evaporation models directly and against the experimental data, we construct a numerical code for solving eq. (1). Our numerical code is the extension of the code used in [20]. Figure 4a) shows the evolution of the drop volume as a function of time. We find good agreement between the experimental results and the NEOS model for a DIW drop considered here. The lens model, on the other hand, overestimates the volume loss due to evaporation. Hence, at least for a DIW drop evaporating on Si substrate, Fig. 4a) indicates that the NEOS model predicts better the volume loss compared to the lens model. We note that the possible sources of the difference between these

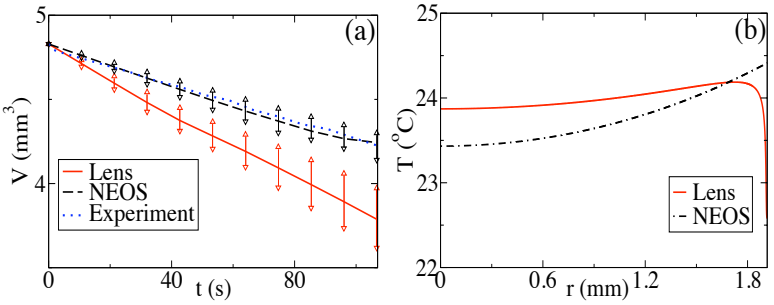

Figure 4: (a) Volume of an evaporating DIW drop: comparison of the models with the experiment. The lines correspond to the mean values of volatility parameters, and the error bars to those obtained using the mean values ± standard deviation. (b) Temperature of the liquid-gas interface predicted by the two models at the final time shown in (a) (using mean values of α and χ).

results and the established ones [7, 10], are that we consider drops which do not experience contact line pinning, and that our drops are significantly larger than those considered in [7]. A combination of these factors may result in a situation where lens model is more favorable. We further discuss these differences elsewhere [17].

Figure 4b) shows, perhaps the most surprising result of this comparison. It indicates that the two models predict qualitatively different temperature profiles along the liquid/gas interface. In the NEOS model, the fact that the heat supplied from the solid is larger than the heat loss due to evaporation leads to an increase of temperature as one moves from the center. On the other hand, the lens model predicts significantly larger evaporative flux in the contact line region, therefore leading to a sharp decrease of temperature there. The former result is consistent with the results obtained using the lens model, and similar parameter values, although under the assumption of a pinned contact line [10, 14]. A curious feature of the lens results shown in fig. 4b) is a 'stagnation point', where the temperature gradient changes sign. A temperature profile with such a maximum could be used for explaining the occurrence of stagnation points in recently recorded experiments [23], although this phenomena, a necessary ingredient for formation of ring-like deposits typical for evaporating colloidal drops, could be based on entirely different physical grounds [9].

We find it intriguing that the results regarding the evolution of drops' volume, radius, and, in particular, the liquid-gas interfacial temperature, produced by the two commonly used evaporation models are so qualitatively different – the resulting Marangoni forces may act in the opposing directions. We hope that the results presented here will encourage more elaborate experiments, particularly those involving direct measurement of the interfacial liquid-gas temperature, an ultimate test for any evaporation model.

Acknowledgment We thank to all the other researchers who set a stage for this work and allowed us to reach current level of understanding of evaporative mechanisms. The contribution of Bud Homsy has been invaluable here, as well as in many other problems in fluid mechanics.

References

[1] R. Blossey. Self-cleaning surfaces - virtual realities. *Nature Materials*, 2:301, 2003.

[2] R.D. Deegan, O. Bakajin, T.F. Dupont, G. Huber, S.R. Nagel, and T.A. Witten. Capillary flow as the cause of ring stains from dried liquid drops. *Nature*, 389:827, 1997.

[3] S. J. S. Morris. Contact angles for evaporating liquids predicted and comapred with existing experiments. *J.Fluid Mech.*, 432:1, 2001.

[4] V.S. Ajaev, G.M. Homsy, and S.J.S. Morris. Dynamic response of geometrically constrained vapor bubbles. *J. Colloid Interface Sci.*, 254:346, 2002.

[5] P. Colinet, J.C. Legros, and M.G. Velarde. *Nonlinear dynamics of surface-tension-driven instabilities*. Wiley-VCH, Berlin, 2001.

[6] J. Margerit, M. Dondlinger, and P.C. Dauby. Improved 1.5-sided model for the weakly nonlinear study of Benard-Marangoni instabilities in an evaporating liquid layer. *J. Colloid Interface Sci.*, 290:220–230, 2005.

[7] H. Hu and R.G. Larson. Evaporation of a sessile droplet on a substrate. *J. Phys. Chem. B*, 106:1334, 2002.

[8] Y. O. Popov. Evaporative deposition patterns: Spatial dimensions of the deposit. *Phys. Rev. E*, 71:036313, 2005.

[9] R.D. Deegan, O. Bakajin, T.F. Dupont, G. Huber, S.R. Nagel, and T.A. Witten. Contact line deposits in an evaporating drop. *Phys. Rev. E*, 62:756, 2000.

[10] H. Hu and R. G. Larson. Analysis of the effects of Marangoni stresses on the microflow in an evaporating sessile droplet. *Langmuir*, 21:3972, 2005.

[11] M. Cachile, O. Benichou, C. Poulard, and A.M. Cazabat. Evaporating droplets. *Langmuir*, 18:8070, 2002.

[12] G. Guena, C. Poulard, and A. M. Cazabat. Evaporating drops of alkane mixtures. *Colloids Surf. A*, 298:2, 2007.

[13] B.J. Fischer. Particle convection in an evaporating colloidal droplet. *Langmuir*, 18:60, 2002.

[14] W.D. Ristenpart, P.G. Kim, C. Domingues, J. Wan, and H.A. Stone. Influence of substrate conductivity on circulation reversal in evaporating drops. *Phys. Rev. Lett.*, 99:234502, 2007.

[15] N. Murisic and L. Kondic. How do drops evaporate? cond-mat/08023207, 2008.

[16] A. Oron, S. H. Davis, and S. G. Bankoff. Long-scale evolution of thin liquid films. *Rev. Mod. Phys.*, 69:931, 1997.

[17] N. Murisic and L. Kondic. On modeling evaporation. in preparation, 2008.

[18] A. Prosperetti and M.S. Plesset. Vapour-bubble growth in a superheated liquid. *J. Fluid Mech.*, 85:349, 1978.

[19] V.S. Ajaev. Spreading of thin volatile liquid droplets on uniformly heated surfaces. *J.Fluid Mech.*, 528:279, 2005.

[20] Y. Gotkis, I. Ivanov, N. Murisic, and L. Kondic. Dynamic structure formation at the fronts of volatile liquid drops. *Phys. Rev. Lett.*, 97:186101, 2006.

[21] R.D. Deegan. Pattern formation in drying drops. *Phys. Rev. E*, 61:475, 2000.

[22] N. Murisic. *Instabilities of Evaporative Drops and Films*. PhD thesis, New Jersey Institute of Technology, 2008.

[23] X. Xu and J. Luo. Marangoni flow in an evaporating water droplet. *App. Phys. Lett.*, 91:124102, 2007.